RSC Advances

PAPER

View Article Online
View Journal | View Issue

Cite this: *RSC Adv.*, 2018, **8**, 2410

Self-assembled MoS_2/rGO nanocomposites with tunable UV-IR absorption†

Wei Wang, *[ab] Olesya O. Kapitanova,[c] Pugazhendi Ilanchezhiyan,[b] Sixing Xi,[a] Gennady N. Panin, *[bd] Dejun Fu[e] and Tae Won Kang[b]

Received 15th November 2017
Accepted 20th December 2017

DOI: 10.1039/c7ra12455d

rsc.li/rsc-advances

MoS_2/reduced graphene oxide (rGO) nanocomposites were synthesized using an ultrasonic pretreatment with a single-stage hydrothermal and reduction process. Self-assembled MoS_2 layers in the rGO matrix were obtained. The effect of quantum confinement in the structure, controlled by the degree of reduction of graphene oxide and the size of the 2D MoS_2 nanocrystals, made it possible to obtain tunable optical absorption. MoS_2/rGO layered nanocomposites exhibit a wide UV-IR absorption in the wavelength range from 280 nm to 973 nm, which is attractive for highly efficient multiband solar cells and advanced photonics.

Introduction

Layered two-dimensional materials have attracted considerable interest owing to their outstanding physical and chemical properties. The first and most investigated two-dimensional crystal graphene has excellent mechanical, thermal, electrical, and optical properties[1–5] and is promising in various fields, such as electronics,[6,7] optoelectronics,[8,9] supercapacitors,[10,11] photocatalysis,[12] and biochemical sensors.[13]

Recently, molybdenum disulfide (MoS_2), a layered inorganic compound that is a semiconducting analog of graphene, has attracted much attention due to its noticeable bandgap, suitable for logic applications in electronics, and photonics. The MoS_2 crystal consists of covalently bonded S–Mo–S atoms in the plane. The adjacent layers with a spacing of ~6.5 Å are weakly stacked on the top of each other by van der Waals interactions. The indirect band gap of 1.3 eV for bulk crystal MoS_2 is transformed into a direct band gap of ~1.9 eV for monolayer MoS_2, which is attributed to quantum confinement resulting in changes in hybridization states d- and p_z-electrons of Mo and S atoms, respectively.[14] Remarkable mechanical[15–17] and optoelectrical properties[14] of MoS_2 make it attractive in various fields of energy harvesting and storage such as hydrogen storage,[18,19] photocatalysis,[20] solar cells[21] and ion batteries.[22–25] Weak van der Waals interactions of neighboring MoS_2 layers allow the creation of new composites with unique properties.[26] Hydrothermal/solvothermal synthesis is a cost effective way of growing MoS_2 due to low growth temperature, a simple inexpensive process and mild synthetic conditions suitable for varies substrates, including flexible, large-scale, and selectively structured. The morphology of the MoS_2 crystals can be controlled by pretreating the substrate prior to the growth process by adding an organic solvent such as i-propanol (IPA), acetic acid, L-cysteine, and oleylamine,[22,23,27,28] which play the role of buffering. Structural and morphological compatibility of graphene and MoS_2 allows the use of graphene-like molecules, such as reduced graphene oxide (rGO), carbon nanotubes, *etc.* as a precursor platform in the hydrothermal method for producing layered MoS_2.[23,25,27]

In this work, self-assembled MoS_2/rGO nanocomposites with various structures were obtained using ultrasonic pretreatment with liquid-phase reaction and reduction, which allow controlling the optical absorption of nanocomposites in a wide range of wavelengths.

Experimental

Synthesis of graphene oxide

Graphene oxide (GO) was obtained by a modified Hummer's method.[29,30] In this method, oxidation was combined with a highly efficient method of purifying reaction products. Concentrated sulphuric acid (H_2SO_4, purity 96%, 360 mL) and phosphoric acid (H_3PO_4, purity 69.2%, 40 mL) were placed in a flask with mild stirring. Natural graphite flakes (Aldrich graphite, 3.0 g, purity 99.995 wt%, high density) were added and dispersed in the mixture, followed by the gradual addition of

[a]School of Mathematics & Physics, Hebei University of Engineering, Handan 056038, China. E-mail: wangwei19872010@163.com

[b]Department of Physics, Quantum-functional Semiconductor Research Center, Nano Information Technology Academy, Dongguk University, Seoul 100-715, Republic of Korea. E-mail: g_panin@dongguk.edu

[c]Department of Chemistry, Moscow State University, Leninskie Gory, 1, b.3, 119991, Moscow, Russia

[d]Institute for Microelectronics Technology & High Purity Materials, RAS, 142432 Chernogolovka, Moscow District, Russia. E-mail: panin@iptm.ru

[e]Key Laboratory of Artificial Micro- and Nano-Materials of Ministry of Education, School of Physics and Technology, Wuhan University, Wuhan 430072, China

† Electronic supplementary information (ESI) available. See DOI: 10.1039/c7ra12455d

potassium permanganate ($KMnO_4$, 18.0 g, purity 99%) used as the reducing agent during reaction process. The above mixture was maintained for 36 h at room temperature to release the gas under continuous stirring. The resulting solution is terminated by the addition of an aqueous solution of hydrogen peroxide (H_2O_2, 3 mL, 30 wt%), followed by continuous stirring for 30 minutes. The resulting mixture was then added to an aqueous solution of H_2SO_4 (500 mL, 5 wt%) with stirring for 20 minutes, followed by stirring for 1 hour. The mixture was sifted through two metal standard testing sieves with diameters of 320 μm and 30 μm. The filtrate was centrifuged with 9000 rpm for 20 minutes, and the supernatant was decanted away. The remaining solid material was then washed successively with 400 mL of 30% HCl, 1000 mL of distilled water, and 1000 mL of ethanol. The resulting GO suspension was dried in vacuum at 60 °C.

Synthesis of MoS_2/rGO composite and characterization

MoS_2/rGO nanocomposites with MoS_2 2D crystals in the rGO matrix were prepared by ultrasonic pretreatment with a soft liquid-phase reaction and reduction using sodium molybdate ($Na_2MoO_4 \cdot 2H_2O$), thioacetamide (CH_3CSNH_2, TAA), and GO as starting materials. The CH_3CSNH_2 (TAA, 0.06 g) and 0.5 mg mL^{-1} GO suspension, TAA : GO = 1 : 1 (wt%) (0 mg mL^{-1}; 1 mg mL^{-1}, 1 : 2 (wt%), 1.5 mg mL^{-1}, 1 : 3 (wt%)) were dissolved in a beaker with 20 mL of deionized (DI) water. After ultrasonication for 1 h, $Na_2MoO_4 \cdot 2H_2O$ (0.03 g) was added into the solution. GO sheets containing abundant oxygen functional groups give rise to good dispersion due to the interaction between cations and GO sheets and at the same time lead to a decrease in the interaction between GO sheets and inorganic species owing to their negative charge.[31] After vigorous stirring and ultrasonication of obtained dispersion both for 30 min, the pH value of the mixture was mildly modified to neutral by adding 1 M NaOH drop by drop. The obtained solution was used to grow MoS_2/rGO composite by the hydrothermal technique. The blended solution was transferred into a 100 mL Teflon-lined stainless steel autoclave, followed by heating at 220 °C for 24 h. During hydrothermal process, GO was reduced using NaOH as a reducing agent to rGO with simultaneous dispersion of MoS_2 and rGO nanosheets. The black precipitates of MoS_2/rGO composites were first retrieved from the mixed solution after natural cooling down to room temperature and then were washed by centrifugation (9000 rpm for 20 min) with 200 mL of acetone, 200 mL of methanol, and 200 mL of DI water for more than five times decanting away the supernatant. Then obtained product was dried at 80 °C for 6 h in a vacuum oven. The black powder of MoS_2/rGO composite of different composition was dispersed in IPA by vigorously sonication for 1 h to produce the homogenous solution. Ultrasonication was carried out through a point probe (Vibra cell) and a high-speed centrifuge (Eppendorf 5804). The suspension was separated out by different centrifugation speed. The obtained suspension of MoS_2/rGO composite was spin-coated on the SiO_2/Si substrate. The obtained composites were annealed with a rapid thermal annealing at 800 °C for 5 min in a gas stream of 200 sccm (H_2/N_2 = 1 : 4).

The crystalline structure of the synthesized MoS_2/rGO composites was analyzed by field emission scanning electron microscopy (FESEM, S4800), X-ray diffraction techniques (XRD, Bruker D8 Advance) using a Cu Kα radiation (λ = 0.154 nm), high resolution transmission electron microscopy (HRTEM, JEM-2010FEF), and micro-Raman spectrometry (LabRAM HR800, He–Ne laser, 488 nm). The chemical composition of the composites was investigated using X-ray photoelectron spectroscopy (XPS, Escalab 250Xi, Mg Kα excitation), and the XPS spectra were fitted using Gaussian–Lorentzian peak shape and Shirley background subtraction. Optical absorption spectra were recorded using a Carry UV-vis spectrophotometer at room temperature.

Results and discussion

Fig. 1 shows SEM images of MoS_2/rGO nanocomposites with different ratios. The as-grown MoS_2 (TAA : GO = 1 : 0) shows significantly aggregated spherical particles with a diameter of ~700 nm (Fig. 1(a)). However the addition of GO leads to a decrease in the diameter and degree of aggregation of the particles (TAA : GO = 1 : 1) (Fig. 1(b)). MoS_2 spheres are not observed for MoS_2/rGO dispersions with TAA : GO = 1 : 2 and 1 : 3, indicating that rGO derived from GO acts as a dispersant platform, efficiently reducing the aggregation of MoS_2 and forming during the hydrothermal process, self-assembled MoS_2/rGO layered structures. Annealing changes slightly the morphology of the as-grown structure (Fig. 1S†).

Fig. 2a shows X-ray diffraction patterns of MoS_2/rGO composites with different TAA/GO ratios. The diffraction peaks at 2θ = 14.1, 29.5, 32.9, 33.8, 39.5, 43.3, 49.4, 58.4, and 59.2 degree are in good agreement with the (002), (004), (100), (101), (103), (006), (105), (110) and (008) planes of the hexagonal MoS_2 phase (JCPDS 75-1539), respectively.[32,33] The (002) peak, detected in the grown MoS_2, indicates well-stacked layers along the (002) direction.[31] A wide diffraction peak is also observed at 2θ = 24.3 degrees, which is explained by the (002) plane of graphene layers corresponding to *d*-spacing of about 0.34 nm.[22,24,25] The peak (002) of MoS_2 gradually decreases and, finally, disappears in MoS_2/rGO composites with increasing rGO/MoS_2 ratio. This indicates a reduction of MoS_2 in the structure stacked along the *c*-axis to the MoS_2 monolayer in composites with a high GO/TAA ratio (TAA : GO = 1 : 3).

The composites were also examined using high-resolution transmission electron microscopy (HRTEM). Typical HRTEM images of the MoS_2 and MoS_2/rGO composite (1 : 2) are shown in Fig. 3. MoS_2 is well-stacked into more than 5 layers with interlayer distances of 0.62 and 0.22 nm, which are consistent with (002) and (103) 2H-MoS_2 planes, respectively. However, the MoS_2/rGO composite (1 : 2) shows self-assembling 1–2 layers of MoS_2 on the rGO. The distances between the MoS_2 layers of 0.316 and 0.208 nm correspond to the (004) and (006) planes, respectively.

Raman spectra of the nanocomposites (Fig. 2(b) and S2†) show the peaks at ~382 and ~405 cm^{-1}, which correspond to E^1_{2g} and A_{1g} modes of H-MoS_2 and characterize the vibration of sulfides in the in-planar and the vertical-plane in the *c*-axis

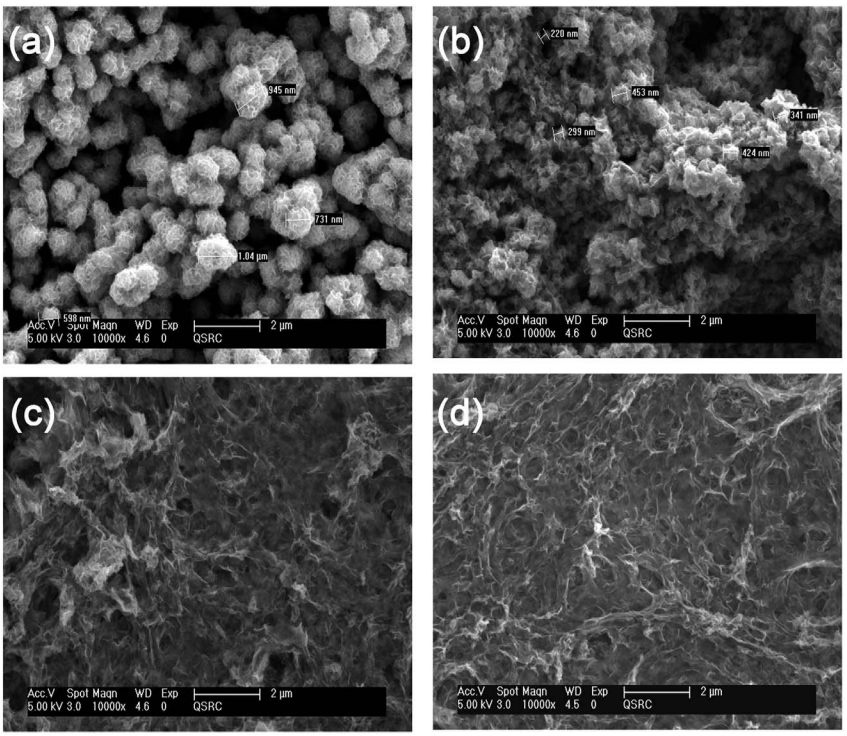

Fig. 1 SEM images of the grown MoS_2/rGO with the ratio (a) (1 : 0), (b) (1 : 1), (c) (1 : 2) and (d) (1 : 3).

directions, respectively.[15,32,34] Two additional peaks at ~1345 and ~1578 cm^{-1} are assigned to the D and G bands of the rGO, which are attributed to the phonon vibration on defects and the sublattice A against the sublattice B (E_{2g} symmetry) in the graphitic layers,[35] respectively, confirming the coexistence of the rGO and MoS_2 in the composites.[36,37] The Raman features of

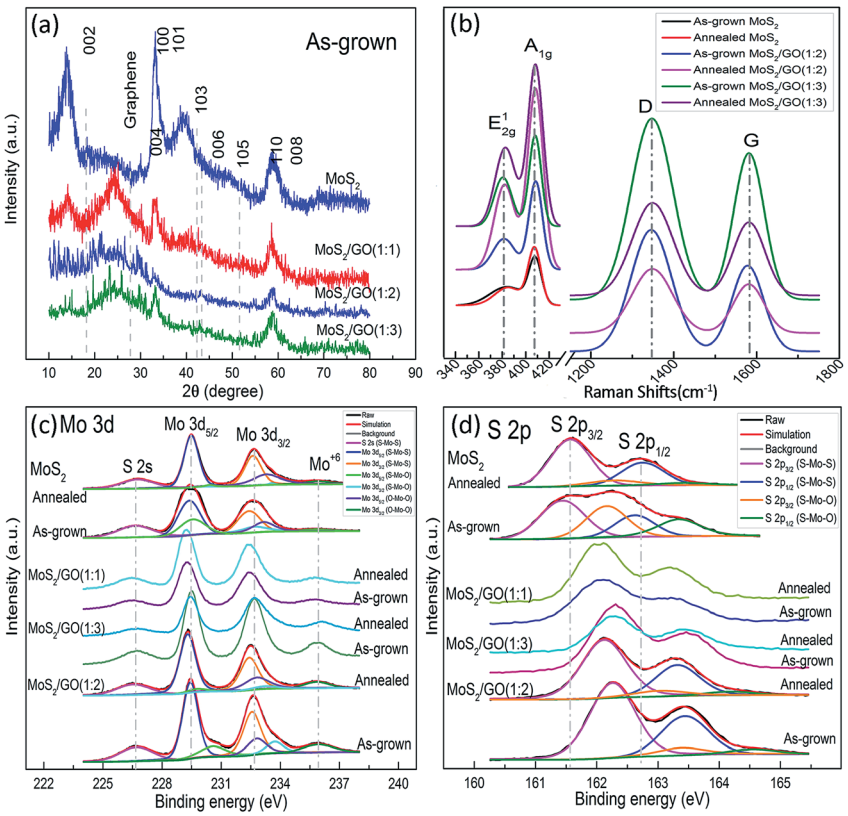

Fig. 2 XRD patterns (a), Raman (b) and XPS (c, d) spectra of MoS_2/rGO with different MoS_2/GO ratios for Mo 3d (c) and S 2p (d).

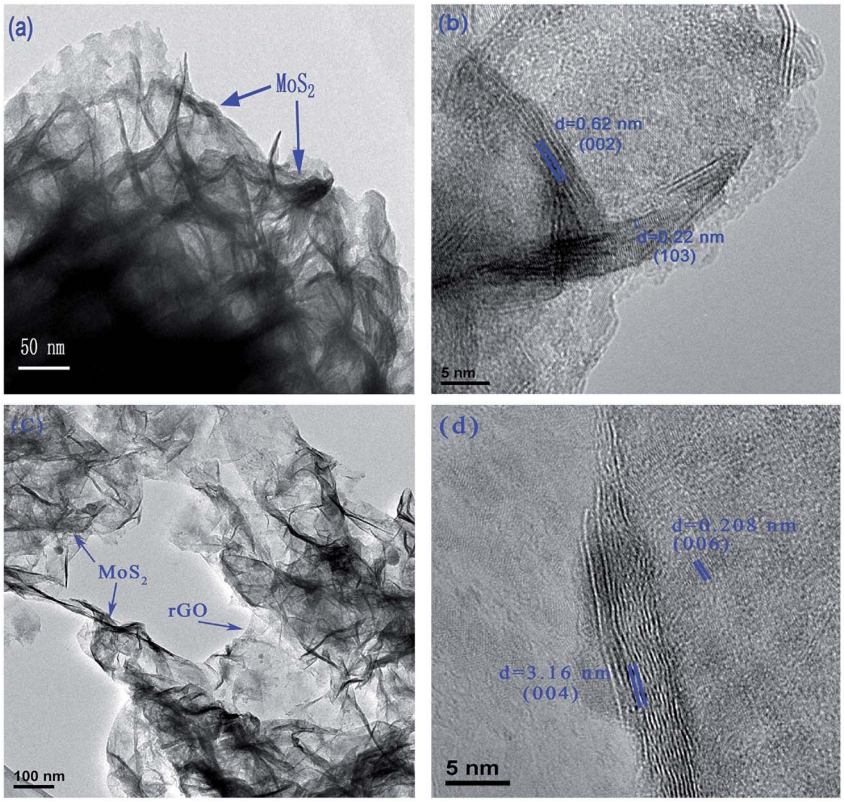

Fig. 3 Typical HRTEM images of MoS_2 (a and b) and MoS_2/rGO (1 : 2) (c and d) composite.

the samples are summarized in Table 1 and S1.† In addition to the blue-shift of the E^1_{2g} and red-shift of the A_{1g}, intriguing degenerate characteristics in full width at half maximum (FWHM) and striking down-shifting of area ratio of E^1_{2g} and A_{1g} modes (I_E/I_A) of MoS_2 were observed with increasing GO. This can be attributed to weak van der Waals forces between the adjacent layers, a decrease in the restoring forces in the vertical direction, the long-range Coulomb interlayer interactions and stacking-induced changes of the intralayer bonding.[34] Elevated temperature of annealing also can effect on crystal reconstruction, intralayer bonding and lattice dynamics. The thickness of MoS_2 layers can be quantitatively confirmed by shifting of E^1_{2g} and A_{1g} modes in frequency (ΔE).[14,34] The values of ΔE decrease with decreasing TAA/GO ratio, which are in good agreement with the data of XRD and HRTEM confirming that the one two layer MoS_2 is self-organizes on rGO. Shifting the G and D bands for composites with increasing GO, could be caused by the stabilizing sulfide in the hydrothermal process and the interaction between MoS_2 and rGO (Table S2†). The intensity ratio G and D (I_G/I_D), used as a factor in determining the quality of the graphene-like material is in the range from 0.5 to 0.6, indicating significant lattice distortions after the reduction of GO in the hydrothermal process. After annealing, the I_G/I_D ratio is increased by further reducing the GO.

The XPS spectra of Mo 3d and S 2p (Fig. 2(c) and (d)) show the peaks centered at ~229.3 and ~232.5 eV, which correspond to the doublet of Mo $3d_{5/2}$ and Mo $3d_{3/2}$, and reveal that typical Mo^{4+} state is predominant in prepared samples. A slight

Table 1 XPS and Raman data of MoS_2 and MoS_2/rGO composites

		XPS (at%)				Raman (cm^{-1})		
Specimen		S/Mo	S–Mo–S	S–Mo–O	O–Mo–O	I_E/I_A	ΔE	I_G/I_D
MoS_2	As-grown	1.5	69.7	18.6	11.7	1.18	26.5	—
	Annealed	2.1	61.1	1.2	21.9	0.97	26.2	—
MoS_2/rGO (1 : 1)	As-grown	1.4	72.8	9.3	17.9	1.01	24.7	0.6
	Annealed	1.5	75.0	5.9	19.1	0.83	23.2	0.5
MoS_2/rGO (1 : 2)	As-grown	1.5	64.8	17.1	18.1	0.87	22.5	0.6
	Annealed	1.6	72.7	5.5	21.8	0.64	21.9	0.6
MoS_2/rGO (1 : 3)	As-grown	1.3	58.6	12.3	29.1	0.8	21.8	0.6
	Annealed	1.8	59.3	5.3	35.4	0.66	21.4	0.6

amount of Mo^{6+} (~236.0 eV) state still appears and increases with addition of GO, which is due to the oxidization of MoS_2 by oxygen resulted from reduction of GO. The Mo $3d_{5/2}$ peak can be divided into three peaks centered at 229, 230, and 232 eV, corresponding to Mo in S–Mo–S, S–Mo–O, and O–Mo–O, respectively. The XPS spectra of S display the binding energy at 226.4, 162.1, and 163.3 eV, which are assigned as S 2s, S $2p_{3/2}$ and S $2p_{1/2}$, respectively. The S $2p_{3/2}$ peak can be divided into two peaks centered at 162 and 163 eV, corresponding to S–Mo–S and S–Mo–O bonds (Table 1 and S2†). Reduced GO plays a role of a scalable precursor platform for adjusting the synthesis conditions for the self-assembly of MoS_2 layers in GO. Properly used amount of rGO increases the intensity of the S–Mo–S bands. At high oxygen concentration the intensities of the S–Mo–S bands decrease, which results in indicating a lower yield of MoS_2. The C 1s spectra prove the process of reducing the GO supplying oxygen (Fig. S3b and Table S3†). After annealing, the intensities of O–Mo–O and S–Mo–O bands increased and decreased, respectively, while the intensities of the S–Mo–S bands changed slightly, which can be explained by a phase transition from $Mo_2S_xO_{1-x}$ to MoO_3. Annealing improved the quality of the crystals and removed the reaction residues. The atomic ratio of S and Mo after annealing of composites was in the range from 1.5 to 2.1.

The mechanism of formation of the self-assembled MoS_2/rGO composite is illustrated in Fig. 4. Cations $(CSNH_2)^+$ (as TA^+) are adsorbed onto the surface of GO sheets during the mixing process and ultrasonic treatment through strong electrostatic forces, resulting in the changing the GO charge to positive. Positive charge sheets of GO ensure overcoming the repulsion of the charges between GO and MoO_4^{2-}. Thus, a suspension of positively charged sheets of GO with adsorbed TA^+ was obtained. When $Na_2MoO_4 \cdot 2H_2O$ is added to the resulting solution, MoO_4^{2-} can be adsorbed on the TA^+–GO single sheets surface to reconstitute the MoO_4^{2-}–TA^+–GO sheet complex.[38,39] The hydrothermal process results in the GO being reduced to rGO, forming a self-assembled MoS_2/rGO composite.

Control of the degree of reduction of graphene oxide allows the creation of super lattices structures with quantum confinement of electrons. Reduction of graphene oxide to rGO with a small band gap (<1.3 eV) would confined the electrons in rGO between the layers of molybdenum disulfide $E_g = 1.3$ eV. Reducing GO to rGO with a bandgap larger than the bandgap of a single layer of molybdenum disulfide (1.8 eV) or its multilayers (1.3 eV), leads to localization of electrons in the layers of molybdenum disulfide. Nanocomposites with tunnel barriers may form local super lattices with different bandgap. Thus, the size effect can adjust the wavelengths of absorption of the nanocomposite.

To confirm the tunability of the optical properties of the MoS_2/rGO nanocomposite, UV absorption spectroscopy was used. The absorption spectrum of rGO shows a peak at about 280 nm, which originates from the π–π* transitions in the aromatic C–C bonds of the reduced graphene oxide[40–42] (Fig. 5a). The MoS_2 absorption spectrum shows four characteristics peaks of around 400–500 nm and 600–700 nm (Fig. 5b). The peaks at 608 and 670 nm corresponds to the exciton peaks of the MoS_2 arising from the *K* point of the Brillouin zone.[43] The peaks at 405 and 452 nm indicate a reduction in the 2H phase of MoS_2.[44] The absorption spectra of MoS_2/rGO composites obtained at different formation conditions show six characteristic peaks located at 250–300 nm, 400–500 nm, 600–700 nm and 973 nm

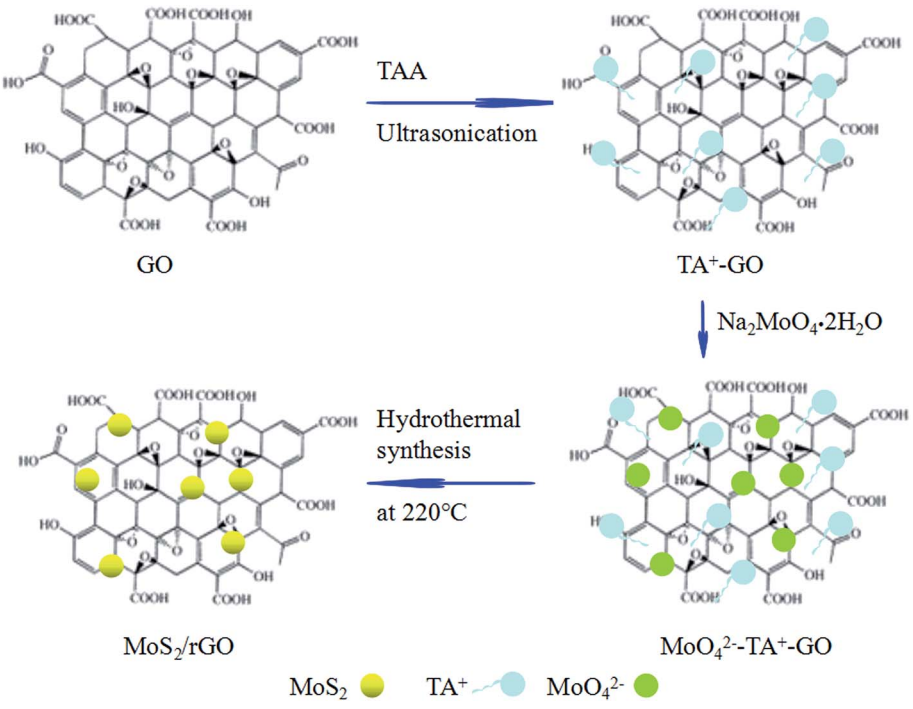

Fig. 4 Schematic illustration of the formation of a self-assembled MoS_2/rGO composite by sonication-assisted hydrothermal method.

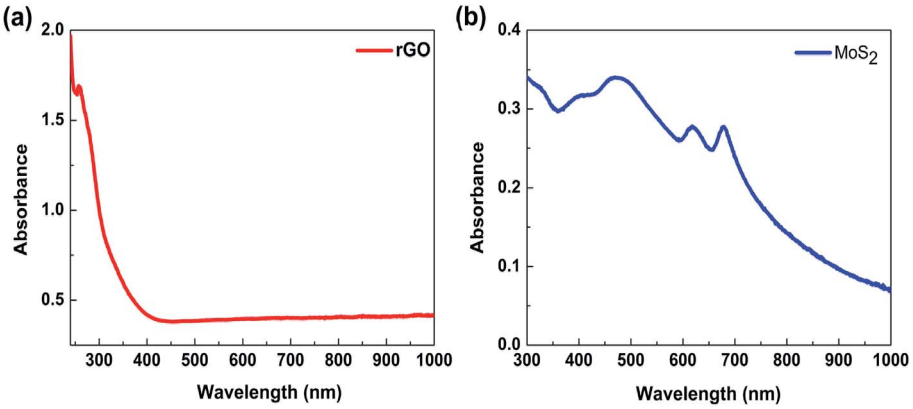

Fig. 5 Absorption spectra of rGO (a) and few layer MoS_2 nanosheets (b).

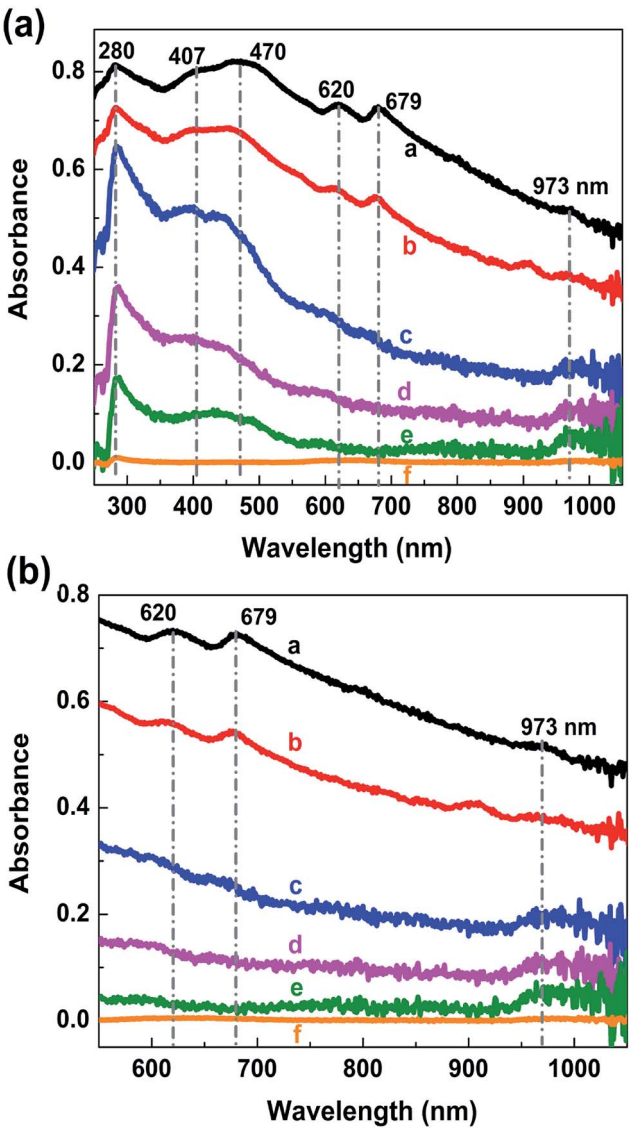

Fig. 6 The absorption spectra of MoS_2/rGO composites from ultraviolet to infrared region (a) and from red to infrared region (b), obtained at different centrifugation speeds: a-3500 rpm, b-5000 rpm, c-6500 rpm, d-8000 rpm, e-9500 rpm, f-11 000 rpm.

(Fig. 6a). It is interesting to note that in the case of MoS_2/rGO nanocomposites, the peak at 280 nm associated with rGO red-shifts to 285 nm gradually with increasing centrifugation rate, indicating an increase in the π-electron concentration with reduction of sp^3 graphene oxide to sp^2-hybridization of carbon atoms.[40–42] For a smaller size of nanocrystals, the self-assembly process results in a more efficient reduction of GO due to possible charge transfer in MoS_2/rGO nanocomposites. In addition, with increasing the centrifugation speed the exciton peaks related to MoS_2 at around 679 nm and 620 nm show a blue shift followed by a decrease in intensity. This behavior in good agreement with the quantum confinement effect,[45] since the size of MoS_2 decreases with increasing centrifugation speed. Interestingly, the absorption spectra of the nanocomposites showed the peak of about 973 nm (1.27 eV), which could be related to the strongly reduced GO (G). This peak is also blue shifted with increasing centrifugation speed and can be explained by the quantum confinement effect in G quantum dots. The obtained results show that the absorption of the MoS_2/rGO nanocomposites can be adjusted over a wide range from ultraviolet to infrared light by using differently reduced GO and MoS_2 flakes of various sizes and thickness. MoS_2/GO nanocomposites with a wide adjustable absorption of light have a great potential for their use in high performance multi-band solar cells and advanced photonics.[46]

Conclusions

MoS_2/rGO nanocomposites were synthesized using ultrasonic pretreatment with a single-stage hydrothermal and reduction process. Self-assembled MoS_2 single layers in the rGO matrix were obtained. The nanocomposites, controlled by the degree of reduction of graphene oxide and the size of MoS_2 nanocrystals, exibit tunable optical absorption in a wide UV-IR wavelength range from 280 nm to 973 nm.

Conflicts of interest

There are no conflicts to declare.

Acknowledgements

This work was supported by the National Natural Science Foundation of China under grant 11405117, the International Program of the Ministry of Science and Technology of China under grant 2015DFR00720 and the National Research Foundation (NRF) of Korea grant funded by the Korea government (MSIP) (No. 2015-066177) and under the framework of international cooperation program managed by NRF of Korea (No. 2015K2A1C2067880 and S-2015-A0173-00005), as well as by Basic Science Research Program through NRF funded by the Ministry of Education (No. 2017R1D1A1B03035102) and the Russian Foundation for Basic Research (RFBR No. 16-33-60229).

Notes and references

1 K. S. Novoselov, A. K. Geim, S. V. Morozov, D. Jiang, Y. Zhang, S. V. Dubonos, I. V. Grigorieva and A. A. Firsov, *Science*, 2004, **306**, 666–669.
2 J. W. Jiang, J. S. Wang and B. W. Li, *Phys. Rev. B: Condens. Matter Mater. Phys.*, 2009, **80**, 113405–113408.
3 R. Murali, Y. Yang, K. Brenner, T. Beck and J. D. Meindl, *Appl. Phys. Lett.*, 2009, **94**, 243114–243116.
4 A. A. Balandin, S. Ghosh, W. Bao, I. Calizo, D. Teweldebrhan, F. Miao and C. N. Lau, *Nano Lett.*, 2008, **8**, 902–907.
5 D. E. Sheehy and J. Schmalian, *Phys. Rev. B: Condens. Matter Mater. Phys.*, 2009, **80**, 193411–193414.
6 F. Schwierz, *Nat. Nanotechnol.*, 2010, **5**, 487–496.
7 C. R. Dean, A. F. Young, I. Meric, C. Lee, L. Wang, S. Sorgenfrei, K. Watanabe, T. Taniguchi, P. Kim, K. L. Shepard and J. Hone, *Nat. Nanotechnol.*, 2010, **5**, 722–726.
8 F. Bonaccorso, Z. Sun, T. Hasan and A. C. Ferrari, Graphene Photonics and Optoelectronics, *Nat. Photonics*, 2010, **4**, 611–622.
9 N. M. Gabor, J. C. W. Song, Q. Ma, N. L. Nair, T. Taychatanapat, K. Watanabe, T. Taniguchi, L. S. Levitov and P. Jarillo-Herrero, *Science*, 2011, **334**, 648–652.
10 Y. Zhu, S. Murali, M. D. Stoller, K. J. Ganesh, W. Cai, P. J. Ferreira, A. Pirkle, R. M. Wallace, K. A. Cychosz, M. Thommes, D. Su, E. A. Stach and R. S. Ruoff, *Science*, 2011, **332**, 1537–1541.
11 Y. Sun, Q. Wu and G. Shi, *Energy Environ. Sci.*, 2011, **4**, 1113–1132.
12 Q. Xiang, J. Yu and M. Jaroniec, *Chem. Soc. Rev.*, 2012, **41**, 782–796.
13 J. D. Fowler, M. J. Allen, V. C. Tung, Y. Yang, R. B. Kaner and B. H. Weiller, *ACS Nano*, 2009, **3**, 301–306.
14 Q. H. Wang, K. Kalantar-Zadeh, A. Kis, J. N. Coleman and M. S. Strano, *Nat. Nanotechnol.*, 2012, **7**, 699–712.
15 A. Castellanos-Gomez, M. Poot, G. A. Steele, H. S. J. van der Zant, N. Agraït and G. Rubio-Bollinger, *Adv. Mater.*, 2012, **24**, 772–775.
16 S. Bertolazzi, J. Brivio and A. Kis, *ACS Nano*, 2011, **5**, 9703–9709.
17 J.-W. Jiang, Z. Qi, H. S. Park and T. Rabczuk, *Nanotechnology*, 2013, **24**, 435705–43570711.
18 A. M. Seayad and D. M. Antonelli, *Adv. Mater.*, 2004, **16**(910), 765–777.
19 J. Chen, N. Kuriyama, H. Yuan, H. T. Takeshita and T. Sakai, *J. Am. Chem. Soc.*, 2001, **123**, 11813–11814.
20 W. Zhou, Z. Yin, Y. Du, X. Huang, Z. Zeng, Z. Fan, H. Liu, J. Wang and H. Zhang, *Small*, 2013, **9**, 140–147.
21 M.-L. Tsai, S.-H. Su, J.-K. Chang, D.-S. Tsai, C.-H. Chen, C.-I. Wu, L.-J. Li, L.-J. Chen and J.-H. He, *ACS Nano*, 2014, **8**, 8317–8322.
22 K. Zhang, H.-J. Kim, X. Shi, J.-T. Lee, J.-M. Choi, M.-S. Song and J. H. Park, *Inorg. Chem.*, 2013, **52**, 9807–9812.
23 K. Chang and W. Chen, *ACS Nano*, 2011, **5**, 4720–4728.
24 K. Chang and W. Chen, *Chem. Commun.*, 2011, **47**, 4252–4254.
25 K. Chang, W. Chen, L. Ma, H. Li, H. Li, F. Huang, Z. Xu, Q. Zhang and J.-Y. Lee, *J. Mater. Chem.*, 2011, **21**, 6251–6257.
26 A. K. Geim and I. V. Grigorieva, *Nature*, 2013, **499**, 419–425.
27 H. Tao, K. Yanagisawa, C. Zhang, T. Ueda, A. Onda, N. Li, T. Shou, S. Kamiya and J. Tao, *CrystEngComm*, 2012, **14**, 3027–3032.
28 C. Altavilla, M. Sarno and P. Ciambelli, *Chem. Mater.*, 2011, **23**, 3879–3885.
29 D. C. Marcano, D. V. Kosynkin, J. M. Berlin, A. Sinitskii, Z. Sun, A. Slesarev, L. B. Alemany, W. Lu and J. M. Tour, *ACS Nano*, 2010, **4**, 4806–4814.
30 G. N. Panin, O. O. Kapitanova, S. W. Lee, A. N. Baranov and T. W. Kang, *Jpn. J. Appl. Phys.*, 2011, **50**, 070110–070115.
31 Z. Wang, T. Chen, W. Chen, K. Chang, L. Ma, G. Huang, D. Chen and J. Y. Lee, *J. Mater. Chem. A*, 2013, **1**, 2202–2210.
32 K.-K. Liu, W. Zhang, Y.-H. Lee, Y.-C. Lin, M.-T. Chang, C.-Y. Su, C.-S. Chang, H. Li, Y. Shi, H. Zhang, C.-S. Lai and L.-J. Li, *Nano Lett.*, 2012, **12**, 1538–1544.
33 I. Zafiropoulou, M. S. Katsiotis, N. Boukos, M. A. Karakassides, S. Stephen, V. Tzitzios, M. Fardis, R. V. Vladea, S. M. Alhassan and G. Papavassiliou, *J. Phys. Chem. C*, 2013, **117**, 10135–10142.
34 C. Lee, H. Yan, L. E. Brus, T. F. Heinz, J. Hone and S. Ryu, *ACS Nano*, 2010, **4**, 2695–2700.
35 L. M. Malard, M. A. Pimenta, G. Dresselhaus and M. S. Dresselhaus, *Phys. Rep.*, 2009, **473**, 51–87.
36 A. C. Ferrari, J. C. Meyer, V. Scardaci, C. Casiraghi, M. Lazzeri, F. Mauri, S. Piscanec, D. Jiang, K. S. Novoselov, S. Roth and A. K. Geim, *Phys. Rev. Lett.*, 2006, **97**, 187401–187404.
37 M. A. Pimenta, G. Dresselhaus, M. S. Dresselhaus, L. G. Cançado, A. Jorio and R. Saito, *Phys. Chem. Chem. Phys.*, 2007, **9**, 1276–1290.
38 X. C. Dong, X. W. Wang, J. Wang, H. Song, X. G. Li, L. H. Wang, M. B. Chan-Park, C. M. Li and P. Chen, *Carbon*, 2012, **50**, 4865–4870.
39 X. Wang, Q. Wang, Q. Wang, F. Gao, F. Gao, Y. Yang and H. Guo, *ACS Appl. Mater. Interfaces*, 2014, **6**, 11573–11580.
40 R. Ortega-Amaya, Y. Matsumoto, A. Flores-Conde, M. A. Pérez-Guzmán and M. Ortega-López, *Mater. Res. Express*, 2016, **3**, 105601–105608.
41 J. Shang, L. Ma, J. Li, W. Ai, T. Yu and G. G. Gurzadyan, *Sci. Rep.*, 2012, **2**, 792–799.

42 O. Akhavan, E. Ghaderi, S. Aghayee, Y. Fereydooni and A. Talebi, *J. Mater. Chem.*, 2012, **22**, 13773–13781.
43 Y. Yao, L. Tolentino, Z. Yang, X. Song, W. Zhang, Y. Chen and C.-P. Wong, *Adv. Funct. Mater.*, 2013, **23**, 3577–3583.
44 G. Eda, H. Yamaguchi, D. Voiry, T. Fujita, M. Chen and M. Chhowalla, *Nano Lett.*, 2011, **11**, 5111–5116.
45 Z. X. Gan, L. Z. Liu, H. Y. Wu, Y. L. Hao, Y. Shan, X. L. Wu and P. K. Chu, *Appl. Phys. Lett.*, 2015, **106**, 233113–233117.
46 X. Fu, P. Illanchezhiyan, G. M. Kumar, H. D. Cho, L. Zhang, A. S. Chan, D. J. Lee, G. N. Panin and T. W. Kang, *Nanoscale*, 2017, **9**, 1820–1826.